Journal of
Applied Crystallography
ISSN 0021-8898

Received 16 August 2006
Accepted 9 January 2007

A comparison of methods for the measurement of the particle-size distribution of magnetic nanoparticles

R. C. Woodward,[a]* J. Heeris,[a] T. G. St. Pierre,[a] M. Saunders,[b] E. P. Gilbert,[c] M. Rutnakornpituk,[d] Q. Zhang[e] and J. S. Riffle[e]

[a]School of Physics, The University of Western Australia, Australia, [b]Centre for Microscopy and Microanalysis, The University of Western Australia, Australia, [c]Bragg Institute, Australian Nuclear Science and Technology Organisation, Australia, [d]Department of Chemistry, Naresuan University, Thailand, and [e]Department of Chemistry, Virginia Polytechnic Institute and State University, USA. Correspondence e-mail: woodward@physics.uwa.edu.au

Recently, interest in magnetic particles, particularly in the nanometre-size range, has increased significantly. The main driving forces behind this interest are both the development of improved synthesis techniques and an increase in the number of potential applications for suitable magnetic nanoparticles. A critical factor of interest in both the synthesis and the development of applications is the particle-size distribution. In this paper, we investigate three common techniques for determining the particle-size distribution of magnetic nanoparticles (electron microscopy, magnetic measurements and small-angle neutron scattering). We compare the distributions determined by each technique for two standard samples and discuss their advantages, disadvantages and limitations.

1. Introduction

A ferrofluid is a colloidal suspension of magnetic nanoparticles, which are generally coated with surfactant or stabilisers to prevent agglomeration. The result is a liquid that can be manipulated using a magnetic field.

Systems of colloidal magnetic particles have been around since the early 1900s but interest blossomed in the 1960s with the production of stable concentrated suspensions of magnetic nanoparticles (Papel, 1965; Khalafalla & Reimers, 1980). These systems of magnetic nanoparticles, now more than a simple scientific curiosity, found a number of significant commercial applications (Rosensweig, 1985; Scherer & Figueiredo Neto, 2005). In recent years, there has been increasing research into magnetic nanoparticulate systems as additional potential applications have been identified. These applications include ferrofluid-based actuators, electromagnetic micropumps, and fluid-based valves and sealing systems (Pérez-Castillejos *et al.*, 2000; Hartshorne *et al.*, 2004; Love *et al.*, 2005). In addition there is also a wide range of potential therapeutic and diagnostic applications such as magnetic targeted drug delivery, magnetic resonance imaging (MRI) contrast enhancement, cell sorting technology, retinal detachment therapy and hypothermia treatment (Pankhurst *et al.*, 2003).

Most applications rely on the particles being superparamagnetic. Superparamagnetism is an interesting magnetic state where there is strong magnetic coupling of the spins within a particle, that would normally result in a ferromagnetic (or ferrimagnetic) state, but the energy barrier between different alignments of the resultant magnetic moment is less then the thermal energy of the particle. This means that the moment for each particle fluctuates between different directions at a rate given by the temperature and the applied magnetic field (Neél, 1955). The result of this is that for a collection of superparamagnetic particles there is no magnetization in the absence of an applied magnetic field. However, on the application of a magnetic field the magnetization, M, is given by:

$$M = c\mu L(\xi) = c\mu[\coth(\xi) - (1/\xi)], \quad (1)$$

where c is the particle concentration, μ is the magnetic moment of the particle and $L(\xi)$ is the Langevin function in which $\xi = \mu H/kT$, where H is the applied magnetic field, k is the Boltzmann constant and T is the temperature in Kelvin. The magnetic moment of the particle μ is related to the particle volume (v) by $\mu = vM_s$ where M_s is the saturation magnetization.

The main advantage of superparamagnetic particles compared to ferromagnetic particles is that ferromagnetic particles tend to agglomerate due to their permanent magnetic dipoles. This agglomeration may cause the suspensions to be unstable or adversely affect the performance of the fluid. A superparamagnetic particle has no permanent magnetic dipole and so suspensions of these particles are stable for long periods of time. In the absence of other factors, the transition between ferromagnetic and superparamagnetic behaviour occurs at a critical particle size, where larger particles are ferromagnetic and smaller particles are superparamagnetic. An estimate of the critical volume for superparamagnetic behaviour (v_c) observed on a timescale of ~100 s can be obtained from equation (2),

$$v_c = 20kT/K, \quad (2)$$

where K is the magnetic anisotropy constant

In the majority of instances, the technological application relies on the generation of a force *via* an applied magnetic field. In general the force is proportional to the magnetic moment of the particle, which itself is proportional to the particle volume. Hence, we have an interesting problem; we wish to maximize the particle size in order to increase the force but do so while keeping it below the critical size for

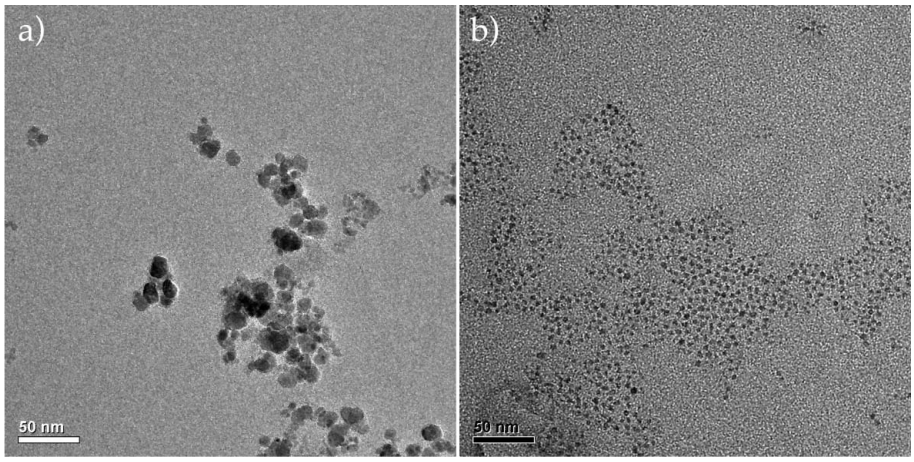

Figure 1
TEM images of the two magnetite samples: (*a*) co-precipitation and (*b*) decomposition.

superparamagnetic behaviour. Hence, in order to optimize the properties of ferrofluid systems we need to be able to measure and control, with some accuracy, the particle-size distribution of magnetic nanoparticulate systems.

Previous work on transmission electron microscopy (TEM), powder X-ray diffraction and nitrogen adsorption measurements has shown that when measuring particles in the nanometre regime the different techniques can give different particle sizes, and that it is very important to understand the advantages, disadvantages and limitations in order to correctly interpret the results (Weibel *et al.*, 2005). In this paper, we will investigate three common techniques for determining the particle-size distribution of magnetic nanoparticles: TEM, magnetic measurements and small-angle neutron scattering (SANS). We will compare the distributions determined by each technique and discuss their advantages, disadvantages and limitations.

2. Synthesis of samples

In this work, we investigated two distinct magnetite-based ferrofluids that represent two of the most commonly observed particle sizes and distribution forms observed in the literature. These ferrofluids were produced using two different techniques.

2.1. Aqueous co-precipitation

The first sample is based on a traditional aqueous co-precipitation technique using polymer stabilisers.

2.1.1. Synthesis of polymer stabilizer. The polymer stabilizer consists of random copolymers of ethylene oxide and propylene oxide (PEO-*co*-PPO) that are used to form triblock copolymers with a urethane centre block (PEO-*co*-PPO-urethane-PEO-*co*-PPO). The PEO-*co*-PPO tail blocks have an average molecular weight of 1808 g mol^{-1} each. The urethane centre blocks contain three carboxylic acid groups that bond to the magnetite surface and have an average molecular weight of 1234 g mol^{-1}. The low molecular weight of the polymers is ideal for forming complexes with the magnetite surface due to low steric hindrance, solution viscosity and rapid diffusion (Zhang *et al.*, 2007).

2.1.2. Synthesis of polymer–magnetite complex. The magnetite complex was synthesized *via* a method similar to that previously described by Harris *et al.* (2003). Iron(III) chloride hexahydrate (1.00 g, 3.70 mmol) and iron(II) chloride tetrahydrate (0.368 g, 1.85 mmol) were charged to a three-neck, 250 ml flask fitted with a mechanical stirrer, pH probe and nitrogen inlet and dissolved in 30 ml of Milli-Q water. Deoxygenated, concentrated aqueous ammonium hydroxide was added with stirring until a pH of 9.5 was reached (~10 ml). The reaction was stirred for a further 30 min and then the polymeric dispersion stabilizer (described above), dissolved in dichloromethane, was added to the reaction and the mixture was rapidly stirred. After a further 30 min of stirring, nitrogen was purged through the reaction until the dichloromethane was evaporated (over 2 h). Finally, the complex was centrifuged for 30 min at 3000 r.p.m. three times to remove aggregates and then dialyzed in a Spectra/Por 6 membrane, MWCO 25000, for 5 days against Milli-Q water. The extraction solvent was refreshed twice a day to remove ammonium salts and any unbound free polymer. The final complex is 30% magnetite and 70% polymer as determined by chemical analysis.

2.2. Organic solution-phase decomposition

The second sample produced by organic solution-phase decomposition results in oleic acid stabilized magnetite nanoparticles in an organic solvent, of either hexane or cyclohexane. The nanoparticles were prepared following the method of Sun & Zeng (2002) with the following modifications. 1.0 g of iron(III) acetylacetonate, 2.0 g of 1,2-dodecanediol, 2.0 ml of oleic acid and 2.0 ml of oleyl amine were dissolved in 20 ml of phenyl ether. The solution was heated to 473 K under nitrogen purging for 30 min and refluxed for 1 h. The solution was then slowly cooled to room temperature. 200 ml of ethanol was added and the solution was centrifuged to precipitate the particles, which were then redispersed in hexane. An additional 200 ml of ethanol was introduced into the dispersion, followed by centrifugation to precipitate the particles. The process was repeated several times in order to completely remove phenyl ether from the dispersion.

3. Particle-size determination

3.1. Transmission electron microscopy

Samples were prepared for TEM by forming a suspension of the particles with a concentration of between 0.1 and 0.01 wt% solids. The dilute sample was then dispersed onto a carbon-coated TEM grid and left to dry for 24 to 48 h. Care must be taken to use clean solvents in order to reduce the formation of dried solids not related to the magnetite particles. The samples were imaged in a Jeol 3000 F field-emission-gun transmission electron microscope at 300 kV and/or a

Jeol 2000FXII transmission electron microscope at 80 kV. Fig. 1 shows images of both (*a*) the co-precipitation and (*b*) the decomposition samples. The particle-size distribution for both samples was determined by manual image analysis of approximately 200 and 500 particles for the co-precipitation and decomposition samples, respectively. Attempts were made to use computer-based image analysis; however, the high level of noise, low contrast and variations in the background intensity make such a technique unreliable.

The particle-size distribution obtained from TEM for the co-precipitation sample has an arithmetic mean particle size and standard deviation of 9.8 and 4.1 nm, respectively, and appears to be a skewed distribution, probably lognormal. For the decomposition sample, the TEM indicates that the distribution is both smaller and narrower than for the co-precipitation sample with an arithmetic mean particle size and standard deviation of 3.6 and 0.9 nm. The size distribution for the decomposition sample appears to be a normal distribution. Both lognormal and normal distributions have been observed previously for magnetic nanoparticles and the form can vary depending on preparation technique (O'Grady & Bradbury, 1983; Berkov *et al.*, 2000).

The advantage of using TEM for determining the particle-size distribution is that one physically observes the particles and obtains information about not only particle size but also morphology. The analysis is simple as no fitting or modelling is required. It is also possible to obtain additional functional information about the particles such as chemical composition, *via* X-ray microanalysis or energy loss spectroscopy, and crystal structure information, *via* electron diffraction or high-resolution imaging (Williams & Carter, 1996).

The presence of aggregates of small crystallites (as seen in Fig. 1a) causes problems in the analysis of particle size as it is debatable whether the particle size should be the aggregate size or the crystallite size (Weibel *et al.*, 2005). Standard TEM sample preparation as used here can result in the formation of aggregates during the drying of the sample that are not necessarily present in the original colloidal suspension. These aggregates can be avoided with special sample preparation techniques such as cryo-TEM (Butter *et al.*, 2003). We have assumed that the majority of aggregates in the co-precipitation sample are artefacts of the TEM sample preparation and so the distribution measured is actually the crystallite distribution.

In addition, TEM imaging, especially when imaging particles just a few nanometres across, has several other disadvantages. As the magnification is increased, obtaining good-quality images with sufficient contrast to accurately identify the particle edges is difficult. Increasing the magnification also limits the field of view, thus reducing the number of particles that can be analysed from a single image. The imaging and analysis can be very time consuming, particularly when the images are unsuitable for computer-based image analysis. Furthermore, both the imaging and any manual image analysis are susceptible to subjective bias. Finally, due to the time-consuming nature of the measurement only a small sample size – fewer than 1000 particles – is usually measured.

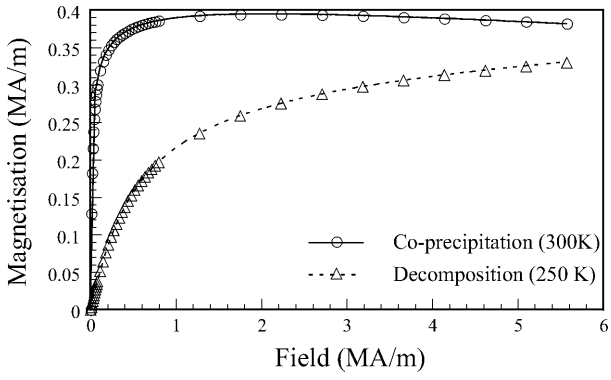

Figure 2
Measured magnetization curves (points) and Langevin function fits to the data (lines). Note: only one temperature is shown for each sample.

3.2. Magnetic measurements (Langevin fitting)

It is possible to determine the particle-size distribution from magnetic measurements. If an ideal sample is measured in the superparamagnetic state then the magnetization is simply given by the integration of the Langevin function [equation (1)] for each particle size in the distribution (Chantrell *et al.*, 1978; O'Grady & Bradbury, 1983). In general, one must specify the form of the distribution in order to generate reasonable fits to the data.[1] For our samples, we assumed a lognormal distribution for the co-precipitation sample and a normal distribution for the decomposition sample consistent with the results from the electron microscopy.

Zero-field cooled–field cooled curves were initially collected using a SQuID magnetometer (Quantum Design 7 Tesla MPMS) in order to determine the maximum blocking temperature, $T_{\rm Bmax}$ (the temperature above which all particles are superparamagnetic). $T_{\rm Bmax}$ for the co-precipitation sample was estimated to be ~450 K, while $T_{\rm Bmax}$ for the decomposition sample was 50 K.

Magnetization curves were collected at 150, 200, 250, 300 and 350 K for the decomposition sample, all above $T_{\rm Bmax}$. These curves were simultaneously fitted to a single particle-size distribution using a least-squares routine containing a numerical integration of the Langevin function, with an additional linear susceptibility term. The final fitted equation had the form

$$M = \int c\mu L(\xi)\, {\rm d}v + \chi_{\rm l} H, \qquad (3)$$

where $\chi_{\rm l}$ is the linear component of susceptibility found in most real samples, owing to paramagnetic and diamagnetic contributions to the moment.

For the co-precipitation sample magnetization curves were collected at 300 and 400 K, temperatures above which the majority of the sample was superparamagnetic but below $T_{\rm Bmax}$. At these temperatures the magnetization curves show a small amount of hysteresis (ferromagnetic behaviour), corresponding to 5 to 1 vol.%, respectively. To fit these curves equation (3) was modified to include an additional ferromagnetic term [given in equation (4)] to account for the small degree of hysteresis (Stearns & Cheng, 1994).

$$M_{\rm ferromagnetic} = \frac{2M_{\rm FS}}{\pi} \arctan\left[\frac{(H \pm H_{\rm c})}{H_{\rm c}} \tan\left(\frac{\pi S}{2}\right)\right], \qquad (4)$$

where $M_{\rm FS}$ is the saturation magnetization of the ferromagnet, $H_{\rm c}$ is the coercive field and S is the loop squareness. Both the 300 and 400 K data were fitted simultaneously to obtain the particle-size distribution.

Representative magnetization curves and fitted Langevin functions for both samples are shown in Fig. 2.

This technique has a number of clear advantages. The measurements are relatively simple and quick, the sample size is large, the data are fitted with a well defined model and, when simultaneously fitted to multiple magnetization curves at different temperatures, can produce distributions with a high level of confidence. The model,

[1] Unless one is able to specify the form of the distribution this is an ill-conditioned problem (*i.e.* small experimental errors cause large non-physical oscillations in the solution) (Berkov *et al.*, 2000).

however, is relatively simple and makes a series of critical assumptions for the Langevin fitting to produce a reliable particle-size distribution. Firstly, it assumes a single magnetic phase where the properties of the magnetic phase do not vary between particles (*e.g.* the saturation magnetization is the same for all particles). The Langevin function also assumes that interactions between particles are insignificant. While this is true in dispersed dilute ferrofluids, this is not necessarily the case in concentrated, aggregated or dried samples.

The major limitation of Langevin fitting is that it is only applicable to superparamagnetic particles. If a significant number of particles are above the critical size for superparamagnetic behaviour (*i.e.* ferromagnetic) then the fitting function cannot predict their magnetic behaviour. Even with the inclusion of the ferromagnetic term of equation (4), the reliability of the fitted results can be called into question given the simplified nature of this ferromagnetic term. For magnetite at 300 K the critical diameter is around 23 nm (based on the anisotropy constant for bulk magnetite). This means that not only is the presence of ferromagnetic particles a problem but if a calculated distribution contains a significant fraction of particles larger than the critical volume then it is unlikely to be realistic distribution.

For the co-precipitation sample the ferromagnetic particles present at the measurement temperatures will generate an error in the determined particle-size distribution for this sample. The particle-size distribution obtained for the co-precipitation sample that was fitted with a lognormal distribution has an arithmetic mean particle size and standard deviation of 12.7 and 8.9 nm, respectively. As mentioned previously this distribution, although useful for qualitative comparison of samples, should probably not be used for quantitative analysis of the particle size due to the presence of ferromagnetic particles. The particle-size distribution for the decomposition sample, with a normal distribution, has an arithmetic mean particle size and standard deviation of 3.7 and 1.1 nm, respectively.

3.3. Small-angle neutron scattering

SANS experiments were performed on the NG3 instrument at the NIST Center for Neutron Research at the National Institute of Standards and Technology, Gaithersburg, Maryland, USA. SANS data were collected on dilute samples with magnetite volume fractions between 0.005 and 0.0002; the total volume fraction including polymer/surfactant is up to an order of magnitude larger. Scattering profiles were measured in D_2O for the co-precipitation sample and in deuterated cyclohexane (C_6D_{12}) for the decomposition sample. All scattering profiles were measured at room temperature in zero field.

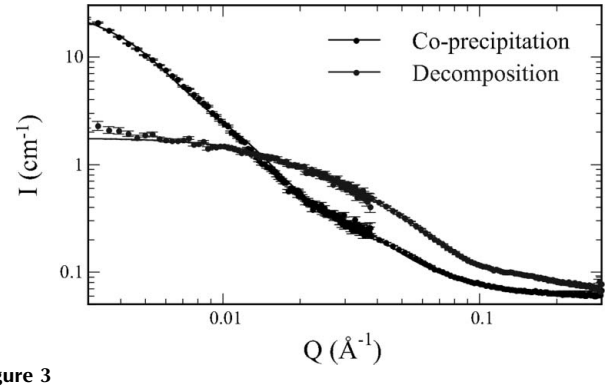

Figure 3
Small-angle neutron scattering curves and fits to the data (Q is the modulus of the scattering vector given by $4\pi\sin\theta/\lambda$ where θ is half the scattering angle and λ is the wavelength of the incident neutrons).

The contrasts used for fitting the data were fixed at the values determined from their chemical composition and bulk densities. The contrast for the magnetite included a contribution from the magnetic scattering after Wiedenmann (2000).

Initially, a polydisperse core-shell model was used to fit the data in which the core size was described by a Schulz distribution with a uniform shell thickness (PolyCore model in *NIST SANS Analysis Macros*, Greenwald & Krzywon, 2005). However, these models were unable to adequately fit the data over the full q range. An inverse approach using the *Irena SAS Macros* (Ilavsky, 2006), which employ regularization techniques (IPG/TNNLS) in order to determine particle-size distributions without having to assume the form of the distribution, was then used to investigate the distributions. Using a polydisperse core-shell model it was shown that both samples could be better described by a bimodal distribution, interpreted to be a distribution of particles and a distribution of aggregates. *SANS Analysis Macros* were then used to fit the data with a sum of two distributions, one a polydisperse core-shell model (PolyCore) representing the particles and a lognormal distribution (LogNormalSphere) representing the aggregates. The starting points for the least-squares fitting procedure were taken from the peaks in the distribution obtained from *Irena SAS Macros*. The shell thickness was fixed at values determined from simultaneous core-shell model fits to multiple-contrast SANS data from polymer micelles for the co-precipitation sample (3.47 nm) (Caba *et al.*, 2007) or from literature values for the length of oleic acid for the decomposition sample (1.02 nm).

The fits to the scattering profiles are shown in Fig. 3. For the co-precipitation sample the arithmetic mean particle size and standard deviation were 17.3 and 6.0 nm, respectively. For the decomposition sample the arithmetic mean particle size and standard deviation were 3.7 and 1.6 nm, respectively, where the fitted volume fraction of the aggregates was between 10 and 30% of the total volume fraction of the samples. The mean size of the aggregates was approximately 100 nm for the co-precipitation sample and 24 nm for the decomposition sample.

SANS has several key advantages for determining the particle-size distribution of nanometre-scale objects. Neutrons are able to probe large sample sizes; the information obtained therefore is representative of the bulk average structure. It is also possible to identify the formation of aggregates in the system through observation of the low-q scattering behaviour. Although not used specifically in this example, it is possible to use contrast variation methods to highlight the scattering from particular components in the system *e.g.* shell thickness or surfactant coating. This can be done using either solvents with variable degrees of deuteration (Jacrot, 1976) or using polarized SANS to generate additional contrast (Wiedenmann, 2000; Wiedenmann *et al.*, 2002).

Access to a SANS facility is generally more difficult than access to TEM or SQuID facilities and requires significant lead time. The results are highly dependent on the model used to fit the data, with a number of models often capable of producing equally good fits to the experimental data. The choice of model and the parameters used then become critical to the quality of the quantitative results. While there is this lack of uniqueness in describing the sample nanostructure, one can gain greater confidence through simultaneous fitting of multiple contrast scattering and simultaneously one can gain significant amounts of information about the system including the thickness and degree of hydration of the surfactant layer (Butter *et al.*, 2004).

There are limitations to the size of particles that can be realistically determined using SANS, particularly for polydisperse systems. For a Schulz distribution with a moderate polydispersity of 0.3, the average

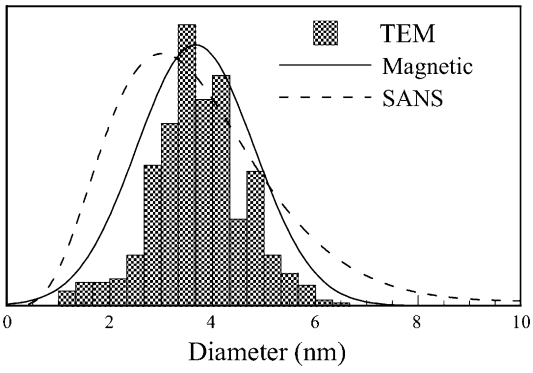

Figure 4
Particle-size distribution determined for the decomposition sample.

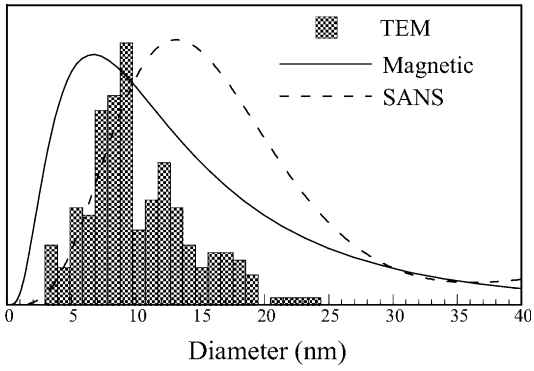

Figure 5
Particle-size distribution determined for the co-precipitation sample.

size that can be realistically determined is within the range 2 to 50 nm. This size range can be extended to larger size by use of USANS (ultra small-angle neutron scattering) and certainly where accurate measurement of aggregates is required this should be considered.

4. Comparison of techniques

There is a high degree of similarity to all three of the particle-size distributions for the decomposition sample (Fig. 4). The TEM and magnetically derived distributions are almost an exact match. The difference between these two and the SANS distribution can be explained in terms of the form of the distribution. The SANS distribution is a Schulz distribution, which is skewed to larger sizes, and may not be entirely suited to this sample. The arithmetic mean particle sizes are 3.6, 3.7 and 3.7 nm for the TEM, magnetic and SANS techniques, respectively, and are equivalent within the experimental errors of the measurements. Previous work by Butter *et al.* (2004) on Fe nanoparticles coated with oleic acid and prepared by thermal decomposition of iron carbonyl found in general good agreement between TEM, magnetic and SANS techniques with a slightly higher difference between the average diameters.

The results for the co-precipitation sample are less clear with a significant variation in both mean particle size and the shape of the distributions (Fig. 5). Both the magnetic and SANS techniques gave wider distributions than that obtained by TEM and it is unclear whether this is an artefact of the magnetic and SANS fitting or a demonstration of the limited sample size and operator bias in TEM. The presence of larger (ferromagnetic) particles in the distribution brings in to question the reliability of the quantitative data from the Langevin fits. When ferromagnetic particles are present it is possible to fit the data with a more rigorous model than used here, such as the sum of a Langevin function and an isotropic Stoner–Wohlfarth model, but this requires either more free parameters in the fit or a detailed understanding of the temperature-dependent properties of the magnetic phase (Bagrets *et al.*, 2004). In the SANS analysis, given the degree of overlap in the bimodal distribution, it is difficult to determine whether the extended width of the distribution is associated with larger particles or results from the presence of smaller aggregates. Similar to what is observed here, Chantrell *et al.* (1978) found that for relatively large particles with broad distributions the particle size determined from TEM was larger than that determined from magnetic measurements.

Both the magnetic and SANS experimental results are particle-volume weighted; as such the contribution from smaller particles becomes less and less significant as the distributions become wider, leading to larger errors in the number-weighted distributions at smaller sizes. This can conflict with TEM, in which the data are collected in terms of the number-weighted distribution.

All three techniques will work better with narrower particle-size distributions, as broad distributions will require more counting in TEM, generate ferromagnetic particles in magnetic measurements and smear out scattering patterns in SANS. TEM imaging is generally easier with larger particles as it is possible to generate higher contrast images that are more amenable to image analysis. The other major advantages of TEM are that no *a priori* knowledge about the distribution shape is required and that variation in the particle morphology can be observed. The magnetic (Langevin fitting) technique is suited to smaller particle sizes below the critical volume for superparamagnetic behaviour, while SANS, particularly when combined with USANS, covers a much wider range of particle sizes. Both the magnetic and SANS techniques are bulk sampling techniques that produce good statistics and can give answers in relatively short time frames. Both techniques can be used with some confidence to qualitatively compare samples. However, they are limited by the need to assume some form for the particle-size distribution and the fits can be subject to experimental artefacts when attempting to determine quantitative results.

5. Conclusions

In this paper the particle-size distributions of two distinctly different magnetite-based ferrofluids were determined using transmission electron microscopy, magnetic measurements and small-angle neutron scattering. All three distributions for the decomposition sample, which had a mean size of 3.7 nm and a distribution width of 1.2 nm, were equivalent within experimental error. The other sample, produced by co-precipitation, had a much larger size and significantly broader distribution. Each of the three techniques gave different particle-size distributions and it is difficult to assert the validity of any particular technique in this case. These results would suggest that it is difficult to quantitatively determine the particle-size distribution for particles with broad distributions. Despite the failure to quantitatively determine the particle size for a broad distribution, all three techniques would appear to be valid for qualitative comparisons.

While all three approaches have their disadvantages, these methods provide complementary information and, when taken together, provide a realistic picture of the particle-size distribution in these technologically important systems.

This research was supported under the Australian Research Council's Discovery funding scheme (project number DP0559333),

The Thailand Research Fund (TRF) and The Ministry of University Affairs (RMU4980006). This work was carried out using facilities at the Centre for Microscopy and Microanalysis, The University of Western Australia, which are supported by University, State and Federal Government funding. The authors also wish to acknowledge the financial support provided by the Department of Education, Science and Training through the Access to Major Research Facilities Program. They also wish to acknowledge NIST Centre for Neutron Research, Gaithersburg, USA, and their staff for support during the SANS measurements, particularly Dr Paul Butler.

References

Bagrets, N., Perov, N., Bagrets, A., Lermontov, A., Pankina, G. & Chernavskii, P. (2004). *J. Magn. Magn. Mater.* **272–276**, 1565–1567.
Berkov, D. V., Görnert, P., Buske, N., Gansau, C., Mueller, J., Giersig, M., Neumann, W. & Su, D. (2000). *J. Phys. D Appl. Phys.* **33**, 331–337.
Butter, K., Bomans, P. H. H., Fredrik, P. M., Vroege, G. J. & Philipse, A. P. (2003). *J. Phys. Condens. Matter*, **15**, S1451–S1470.
Butter, K., Hoell, A., Wiedenmann, A., Petukhov, A. V. & Vroege, G. J. (2004). *J. Appl. Cryst.* **37**, 847–856.
Caba, B. L., Davis, R. M., Carroll, M. R. J., Woodward, R. C., Gilbert, E. P., Zhang, Q. & Riffle, J. S. (2007). In preparation.
Chantrell, R. W., Popplewell, J. & Charles, S. W. (1978). *IEEE Trans. Magn.* **14**, 975–977.
Greenwald, B. & Krzywon, J. (2005). *SANS Analysis Macros Beta for Igor Pro.* NCNR, NIST, Gaithersburg, USA.
Harris, L. A., Goff, J. D., Carmichael, A. Y., Riffle, J. S., Harburn, J. J., St. Pierre, T. G. & Saunders, M. (2003). *Chem. Mater.* **15**, 1367–1377.
Hartshorne, H., Backhouse, C. J. & Lee, W. E. (2004). *Sens. Actuators B*, **99**, 592–600.
Ilavsky, J. (2006). *Irena 2 SAS modeling macros for Igor*. Version 2.11. UNICAT, ANL, Argonne, USA.
Jacrot, B. (1976). *Rep. Prog. Phys.* **39**, 911–953.
Khalafalla, S. E. & Reimers, G. W. (1980). *IEEE Trans. Magn.* **16**, 178–182.
Love, L. J., Jansen, J. F., McKnight, T. E., Roh, Y., Phelps, T. J., Yeary, L. W. & Cunningham, G. T. (2005). *IEEE/ASME Trans. Mechatronics*, **10**, 68–76.
Neél, L. (1955). *Prog. Low Temp. Phys.* **1**, 336–343.
O'Grady, K. & Bradbury, A. (1983). *J. Magn. Magn. Mater.* **39**, 91–94.
Pankhurst, Q. A., Connolly, J., Jones, S. K. & Dobson, J. (2003). *J. Phys. D Appl. Phys.* **36**, R167–R181, and papers cited therein.
Papel, S. S. (1965). *Low viscosity magnetic fluid obtained by the colloidal suspension of magnetic particles*. US Patent 3 215 572.
Pérez-Castillejos, R., Plaza, J. A., Esteve, J., Losantos, P., Acero, M. C., Cané, C. & Serra-Mestres, F. (2000). *Sens. Actuators A*, **84**, 176–180.
Rosensweig, R. E. (1985). *Ferrohydrodynamics*. New York: Cambridge University Press.
Sherer, C. & Figueiredo Neto, A. M. (2005). *Brazil. J. Phys.* **35**, 718–726.
Stearns, M. B. & Cheng, Y. D. (1994). *J. Appl. Phys.* **75**, 6894–6899.
Sun, S. & Zeng, H. (2002). *J. Am. Chem. Soc.* **124**, 8204–8205.
Weibel, A., Bouchet, R., Boulc'h, F. & Knauth, P. (2005). *Chem. Mater.* **17**, 2378–2385.
Wiedenmann, A. (2000). *J. Appl. Cryst.* **33**, 428–432.
Wiedenmann, A., Hoell, A. & Kammel, M. (2002). *J. Magn. Magn. Mater.* **252**, 83–85.
Williams, D. B. & Carter, C. B. (1996). *Transmission electron microscopy: a textbook for materials science*. New York: Plenum Press.
Zhang, Q., Thompson, M. S., Carmichael, A. Y., Caba, B. L., Zalich, M. A., Lin, Y.-N., Mefford, O. T., Davis, R. M. & Riffle, J. S. (2007). Submitted.